


Preequilibrium cluster emission in massive transfer reactions near the Coulomb barrier energyZhao-Qing Feng ^{*}*School of Physics and Optoelectronics, South China University of Technology, Guangzhou 510640, China*

(Received 2 January 2023; revised 21 March 2023; accepted 15 May 2023; published 22 May 2023)

Within the framework of the dinuclear system model, the preequilibrium emission of neutron, proton, deuteron, triton, ^3He , α , ^6Li , ^7Li , ^8Be , and ^9Be in the transfer reactions of $^{12}\text{C} + ^{209}\text{Bi}$, $^{40,48}\text{Ca} + ^{238}\text{U}$, $^{238}\text{U} + ^{238}\text{U}$, and $^{238}\text{U} + ^{248}\text{Cm}$ has been systematically investigated. The production rate, kinetic energy spectra, and emission angular distribution are calculated. It is found that the preequilibrium emission mechanism is associated with the reaction system and beam energy. The preequilibrium cross sections of proton, deuteron, triton, and alpha are comparable in magnitude. The reaction with ^{40}Ca is favorable for the cluster emission in comparison with ^{48}Ca on ^{238}U at the near barrier energy. A broad angular distribution of the preequilibrium cluster is found in the heavy systems $^{238}\text{U} + ^{238}\text{U}$ and $^{238}\text{U} + ^{248}\text{Cm}$. The method is also possible for the weakly bound nuclei induced reactions. Future experiments are discussed for the preequilibrium cluster measurements.

DOI: [10.1103/PhysRevC.107.054613](https://doi.org/10.1103/PhysRevC.107.054613)**I. INTRODUCTION**

The preequilibrium cluster emission in transfer reactions is of significance for the investigation of the correlation of spatial configuration of nucleons, nuclear structure, and reaction dynamics. The cluster structure exists in a nucleus, i.e., ^6Li being composed of α and d , ^8Be being the two α , three α in ^{12}C , surface cluster in heavy nucleus, etc. The cluster is considered to be formed by the overlap of the single-particle wave function. In nuclear reactions, it has been known that the preequilibrium cluster formation is different with the one from the decay of the compound nucleus formed in fusion reactions. The cluster emission provides important information on the single-particle or multiparticle correlation of nuclear states, which has been widely used as powerful nuclear spectroscopic tool [1]. On the other hand, the characteristics of the multinucleon transfer reaction (MNT) and deep inelastic heavy-ion collisions are related to the preequilibrium cluster emission, which has been attempted to create the neutron-rich heavy nuclei, in particular around the neutron shell closure. There are a number of experiments for measuring the kinetic energy spectra, double differential cross section, angular distribution, etc. [2–7]. The deep investigation of the preequilibrium cluster emission in transfer reactions is helpful for exploring the cluster structure of the stable or unstable nuclide, the cluster formation mechanism in nuclear reaction, the synthesis of superheavy nucleus or new isotope, the MNT mechanism, etc. [8–12].

The cluster structure in a nucleus is usually studied by the direct reactions, e.g., the pick-up or knock-out reaction, the breakup reaction, etc. The preequilibrium cluster in the massive transfer reaction is also a direct process, in which the cluster is created before the formation of compound nucleus.

Both the cluster structure and reaction dynamics influence the preequilibrium cluster production. There are many nuclear models for describing the cluster structure and nucleon condensation in a nucleus, in which the cluster preformation probability in the spatial coordinate can be estimated [13–15]. However, the cluster emission in nuclear reaction is very complicated, which is dependent on the space-time evolution, beam energy, cluster structure, etc. A few of reaction models or phenomenological formula are proposed for the preequilibrium particle emission, e.g., the exciton model [16–18], Langevin equations [19], and quantum molecular dynamics model [20]. A sophisticated model is still needed for precisely describing the preequilibrium cluster emission. Both the cluster configuration of collision system and reaction dynamics influence the cluster production, i.e., the kinetic energy spectra and angular distribution.

In this work, the preequilibrium cluster emission in the transfer reactions is to be systematically investigated within the framework of dinuclear system (DNS) model. The article is organized as follows. In Sec. II, we give a brief description of the DNS model for describing the preequilibrium cluster production. In Sec. III, the production cross sections, kinetic energy spectra, and angular distribution of the preequilibrium cluster are analyzed and discussed. Summary and perspective on the cluster emission in the transfer reactions are shown in Sec. IV.

II. BRIEF DESCRIPTION OF THE MODEL

The DNS concept assumes that the colliding system is formed at the touching configuration in nuclear collisions and proposed by Volkov at Dubna for describing the deep inelastic heavy-ion collisions [21]. The typical sticking time is several zeptoseconds. The nucleon exchange and energy dissipation take place once the DNS is formed. The nucleon transfer between the binary fragments is governed by the single-particle

^{*}Corresponding author: fengzqh@scut.edu.cn

Hamiltonian. The DNS model has been used for describing the massive fusion-evaporation mechanism and multinucleon transfer reactions [22–24]. In this work, the preequilibrium cluster production is to be investigated with the model. The cross sections of the preequilibrium clusters ($\nu = n, p, d, t, {}^3\text{He}, \alpha, {}^6,7\text{Li},$ and ${}^8,9\text{Be}$) are estimated as follows:

$$\begin{aligned} \sigma_\nu(E_k, \theta, t) = & \sum_{J=0}^{J_{\max}} \sum_{Z_1=Z_\nu}^{Z_{\max}} \sum_{N_1=N_\nu}^{N_{\max}} \sigma_{\text{cap}}(E_{\text{c.m.}}, J) \int f(B) \\ & \times P(Z_1, N_1, E_1(E_{\text{c.m.}}, J), t, B) \\ & \times P_\nu(Z_\nu, N_\nu, E_k) dB. \end{aligned} \quad (1)$$

Here, E_1 is the excitation energy for the fragment with (Z_1, N_1) , respectively, which is associated with the center-of-mass energy $E_{\text{c.m.}}$ and incident angular momentum J . The maximal angular momentum J_{\max} is taken to be the grazing collision of two colliding nuclei. The preequilibrium cluster might be emitted from all DNS fragments (Z_1, N_1) ranging from the light one (Z_ν, N_ν) to composite system (Z_{\max}, N_{\max}) (Z_{\max} and N_{\max} being the total proton and neutron numbers, respectively). The kinetic energy of cluster is sampled by the Monte Carlo approach within the excitation energy E_1 . The capture cross section is given by $\sigma_{\text{cap}} = \pi \hbar^2 (2J + 1) T(E_{\text{c.m.}}, J) / (2\mu E_{\text{c.m.}})$ with $T(E_{\text{c.m.}}, J) = \int f(B) T(E_{\text{c.m.}}, J, B) dB$. The transmission probability $T(E_{\text{c.m.}}, J, B)$ is calculated by the well-known Hill-Wheeler formula for the light and medium systems. For the heavy systems, for example, ${}^{238}\text{U} + {}^{238}\text{U}$, the classical trajectory approach with a barrier distribution by $T(E_{\text{c.m.}}, J, B) = 0$ and 1 for $E_{\text{c.m.}} < B + J(J + 1)\hbar^2 / (2\mu R_C^2)$ and $E_{\text{c.m.}} > B + J(J + 1)\hbar^2 / (2\mu R_C^2)$, respectively. The μ and R_C denote the reduced mass and Coulomb radius by $\mu = m_n A_p A_t / (A_p + A_t)$ with m_n , A_p , and A_t being the nucleon mass and numbers of projectile and target nuclides, respectively. The distribution function is taken as the Gaussian form $f(B) = \frac{1}{N} \exp[-((B - B_m)/\Delta)^2]$, with the normalization constant satisfying the unity relation $\int f(B) dB = 1$. The quantities B_m and Δ are evaluated by $B_m = (B_C + B_S)/2$ and $\Delta = (B_C - B_S)/2$, respectively. The B_C and B_S are the Coulomb barrier at waist-to-waist orientation and the minimum barrier by varying the quadrupole deformation of the colliding partners.

The nucleon transfer is described by solving a set of microscopically derived master equations by distinguishing protons and neutrons [22,23]. The time evolution of the distribution probability $P(Z_1, N_1, E_1, t)$ for the DNS fragment 1 with proton number Z_1 and neutron number N_1 and excitation energy E_1 is governed by the master equations as follows:

$$\begin{aligned} & \frac{dP(Z_1, N_1, E_1, t)}{dt} \\ & = \sum_{Z'_1} W_{Z_1, N_1; Z'_1, N_1}(t) [d_{Z_1, N_1} P(Z'_1, N_1, E'_1, t) \\ & \quad - d_{Z'_1, N_1} P(Z_1, N_1, E_1, t)] + \sum_{N'_1} W_{Z_1, N_1; Z_1, N'_1}(t) \\ & \quad \times [d_{Z_1, N_1} P(Z_1, N'_1, E'_1, t) - d_{Z_1, N'_1} P(Z_1, N_1, E_1, t)]. \end{aligned} \quad (2)$$

Here the $W_{Z_1, N_1; Z'_1, N_1}$ ($W_{Z_1, N_1; Z_1, N'_1}$) is the mean transition probability from the channel (Z_1, N_1, E_1) to (Z'_1, N_1, E'_1) [or (Z_1, N_1, E_1) to (Z_1, N'_1, E'_1)], and d_{Z_1, N_1} denotes the microscopic dimension corresponding to the macroscopic state (Z_1, N_1, E_1) . The cascade nucleon transfer is considered in the process with the relation of $Z'_1 = Z_1 \pm 1$ and $N'_1 = N_1 \pm 1$. It is noticed that the quasifission of DNS and the fission of heavy fragments are neglected in the dissipation process. Different with the fusion-evaporation reactions [23], the interaction time of the preequilibrium process is at the level of several zeptoseconds. The contribution of quasifission fragments to the preequilibrium cluster formation is very similar to the DNS fragments. The fission process of heavy fragment undergoes the longer temporal evolution in comparison with the preequilibrium dynamics. The interaction time τ_{int} is obtained from the deflection function method [25], which depends on the relative angular momentum and colliding system. On the other hand, the interaction potential is flat at the touching distance and no potential pocket exists in the heavy systems. So the quasifission barrier does not appear. We assume the quasifission and fission do not take place before the dissipation equilibrium. The initial probabilities of projectile and target nuclei are set to be $P(Z_{\text{proj}}, N_{\text{proj}}, E_1 = 0, t = 0) = 0.5$ and $P(Z_{\text{targ}}, N_{\text{targ}}, E_1 = 0, t = 0) = 0.5$. The unitary condition is satisfied during the nucleon transfer process $\sum_{Z_1, N_1} P(Z_1, N_1, E_1, t) = 1$. The motion of nucleons in the interacting potential is governed by the single-particle Hamiltonian [22]. The excited DNS opens a valence space in which the valence nucleons have a symmetrical distribution around the Fermi surface. Only the particles at the states within the valence space are actively at excitation and transfer. The averages on these quantities are performed in the valence space as follows:

$$\Delta \varepsilon_K = \sqrt{\frac{4\varepsilon_K^*}{g_K}}, \quad \varepsilon_K^* = \varepsilon^* \frac{A_K}{A}, \quad g_K = A_K/12, \quad (3)$$

where the ε^* is the local excitation energy of the DNS. The microscopic dimension for the fragment (Z_K, N_K) is evaluated by the valence states $N_K = g_K \Delta \varepsilon_K$ and the valence nucleons $m_K = N_K/2$ ($K = 1, 2$) as

$$d(m_1, m_2) = \binom{N_1}{m_1} \binom{N_2}{m_2}. \quad (4)$$

The transition probability is related to the local excitation energy and nucleon transfer, which are microscopically derived from the interaction potential in valence space as

$$\begin{aligned} W_{Z_1, N_1; Z'_1, N_1} = & \frac{\tau_{\text{mem}}(Z_1, N_1, E_1; Z'_1, N_1, E'_1)}{d_{Z_1, N_1} d_{Z'_1, N_1} \hbar^2} \\ & \times \sum_{ii'} |\langle Z'_1, N_1, E'_1, i' | V | Z_1, N_1, E_1, i \rangle|^2. \end{aligned} \quad (5)$$

The memory time is calculated by

$$\tau_{\text{mem}}(Z_1, N_1, E_1; Z'_1, N_1, E'_1) = \left[\frac{2\pi \hbar^2}{\sum_{KK'} \langle V_{KK} V_{KK'}^* \rangle} \right]^{1/2}, \quad (6)$$

$$\langle V_{KK} V_{KK'}^* \rangle = \frac{1}{4} U_{KK'}^2 g_K g_{K'} \Delta_{KK'} \Delta \varepsilon_K \Delta \varepsilon_{K'} \times \left[\Delta_{KK'}^2 + \frac{1}{6} ((\Delta \varepsilon_K)^2 + (\Delta \varepsilon_{K'}^2)) \right]^{-1/2}. \quad (7)$$

The interaction matrix element is given by

$$\sum_{ii'} |V_{ii'}|^2 = [\omega_{11}(Z_1, N_1, E_1, E_1') + \omega_{22}(Z_1, N_1, E_1, E_1') \delta_{Z_1, N_1, E_1; Z_1, N_1, E_1'} + \omega_{12}(Z_1, N_1, E_1, E_1') \delta_{Z_1, N_1, E_1; Z_1-1, N_1, E_1'} + \omega_{21}(Z_1, N_1, E_1, E_1') \delta_{Z_1, N_1, E_1; Z_1+1, N_1, E_1'}] \quad (8)$$

with the relation of

$$\omega_{KK'}(Z_1, N_1, E_1, E_1') = d_{Z_1, N_1} \langle V_{KK'}, V_{KK'}^* \rangle. \quad (9)$$

A similar process for neutron transfer takes place.

In the relaxation process of the relative motion, the DNS will be excited by the dissipation of the relative kinetic energy. The local excitation energy is determined by the dissipation energy from the relative motion and the potential energy surface of the DNS as

$$\varepsilon^*(t) = E_{\text{diss}}(t) - [U(\{\alpha\}) - U(\{\alpha_{\text{EN}}\})]. \quad (10)$$

The entrance channel quantities $\{\alpha_{\text{EN}}\}$ include the proton and neutron numbers, angular momentum, quadrupole deformation parameters, and orientation angles $Z_P, N_P, Z_T, N_T, J, R, \beta_P, \beta_T, \theta_P,$ and θ_T for the projectile-target system. The excitation energy E_1 for fragment (Z_1, N_1) is evaluated by $E_1 = \varepsilon^*(t = \tau_{\text{int}}) A_1/A$. The energy dissipated into the DNS is expressed as

$$E_{\text{diss}}(t) = E_{\text{c.m.}} - B - \frac{\langle J(t) \rangle (\langle J(t) \rangle + 1) \hbar^2}{2\zeta_{\text{rel}}} - \langle E_{\text{rad}}(J, t) \rangle. \quad (11)$$

Here the $E_{\text{c.m.}}$ and B are the center-of-mass energy and Coulomb barrier, respectively. The radial energy is evaluated from

$$\langle E_{\text{rad}}(J, t) \rangle = E_{\text{rad}}(J, 0) \exp(-t/\tau_r). \quad (12)$$

The relaxation time of the radial motion $\tau_r = 5 \times 10^{-22}$ s and the radial energy at the initial state $E_{\text{rad}}(J, 0) = E_{\text{c.m.}} - B - J_i(J_i + 1)\hbar^2/(2\zeta_{\text{rel}})$. The dissipation of the relative angular momentum is described by

$$\langle J(t) \rangle = J_{\text{st}} + (J_i - J_{\text{st}}) \exp(-t/\tau_J). \quad (13)$$

The angular momentum at the sticking limit $J_{\text{st}} = J_i \zeta_{\text{rel}}/\zeta_{\text{tot}}$ and the relaxation time $\tau_J = 15 \times 10^{-22}$ s. The ζ_{rel} and ζ_{tot} are the relative and total moments of inertia of the DNS, respectively. The initial angular momentum is set to be $J_i = J$ in Eq. (1). The relaxation time of radial kinetic energy and angular momentum dissipation is associated with the friction coefficients in the binary collisions. The values in this work are taken from the empirical analysis in deeply inelastic heavy-ion collisions [25,26].

The potential energy surface (PES) dominates the nuclear transfer and is given by

$$U(\{\alpha\}) = B(Z_1, N_1) + B(Z_2, N_2) - [B(Z, N) + V_{\text{CN}}^{\text{rot}}(J)] + V(\{\alpha\}). \quad (14)$$

Here Z and N are the proton and neutron number of the composite system with $Z_1 + Z_2 = Z$ and $N_1 + N_2 = N$ [24]. The symbol $\{\alpha\}$ denotes the quantities $Z_1, N_1, Z_2, N_2; J, R; \beta_1, \beta_2, \theta_1, \theta_2$. The $B(Z_i, N_i)$ ($i = 1, 2$) and $B(Z, N)$ are the negative binding energies of the fragment (Z_i, N_i) and the compound nucleus (Z, N) , respectively. The $V_{\text{CN}}^{\text{rot}}$ is the rotation energy of the compound system. The β_i represent the quadrupole deformations of the two fragments at ground state. The θ_i denote the angles between the collision orientations and the symmetry axes of deformed nuclei. The interaction potential between fragment (Z_1, N_1) and (Z_2, N_2) includes the nuclear, Coulomb, and centrifugal parts. In the calculation, the distance R between the centers of the two fragments is chosen to be the value at the touching configuration, in which the DNS is assumed to be formed. The tip-tip orientation is chosen in the calculation, which manifests the elongation shape along the collision direction and is favorable for the nucleon transfer to produce the MNT fragments. Shown in Fig. 1 are the PES of DNS fragments and driving potential in the reaction of $^{238}\text{U} + ^{238}\text{U}$. The solid line denotes the driving potential, which means the valley path in the PES. The preequilibrium cluster may be emitted from the DNS fragments, e.g., α from the DNS fragments ^{198}Os and ^{278}Hs , respectively.

The emission probability of preequilibrium cluster $P_v(Z_v, N_v, E_k)$ in the nucleon transfer is calculated by the uncertainty principle within the time step $t \sim t + \Delta t$ and the kinetic energy E_k via

$$P_v(Z_v, N_v, E_k) = \Delta t \Gamma_v / \hbar. \quad (15)$$

Here the time step in the DNS evolution is set to be $\Delta t = 0.5 \times 10^{-22}$ s.

The particle decay widths are evaluated with the Weisskopf evaporation theory as [27,28]

$$\Gamma_v(E^*, J) = (2s_v + 1) \frac{m_v}{\pi^2 \hbar^2 \rho(E^*, J)} \int_0^{E^* - B_v - E_{\text{rot}}} \times \varepsilon \rho(E^* - B_v - E_{\text{rot}} - \varepsilon, J) \sigma_{\text{inv}}(\varepsilon) d\varepsilon. \quad (16)$$

Here, $s_v, m_v,$ and B_v are the spin, mass, and binding energy of the evaporating particle, respectively. The inverse cross section is given by $\sigma_{\text{inv}} = \pi R_v^2 T(\nu)$ with the radius of $R_v = 1.21[(A - A_v)^{1/3} + A_v^{1/3}]$. The penetration probability is set to be unity for neutrons and $T(\nu) = [1 + \exp(2\pi[V_C(\nu) - \varepsilon]/\hbar\omega)]^{-1}$ for charged particles with $\hbar\omega = 5$ and 8 MeV for hydrogen isotopes and other charged particles, respectively. It should be mentioned that the local equilibrium of the DNS is assumed to be formed and the excitation energy $E_i^* = \varepsilon_i^*$ for the i -th fragment is associated with the local excitation energy with the mass table [29]. Shown in Fig. 2 is a comparison of the partial decay widths of neutron, proton, deuteron, triton, $^3\text{He}, \alpha, ^6,7\text{Li},$ and $^8,9\text{Be}$ from the decay of ^{221}Ac , which might be produced in the reaction of $^{12}\text{C} + ^{209}\text{Bi}$ and was performed for the preequilibrium emission of α and ^8Be at Heavy-Ion Research Facility in Lanzhou (HIRFL) [2]. It can be classified three kinds of particle emission according to the magnitude, namely, neutron with the most probable emission, hydrogen isotopes, and α , other charged particles. In the nuclear collisions, the preequilibrium clusters might be emitted from

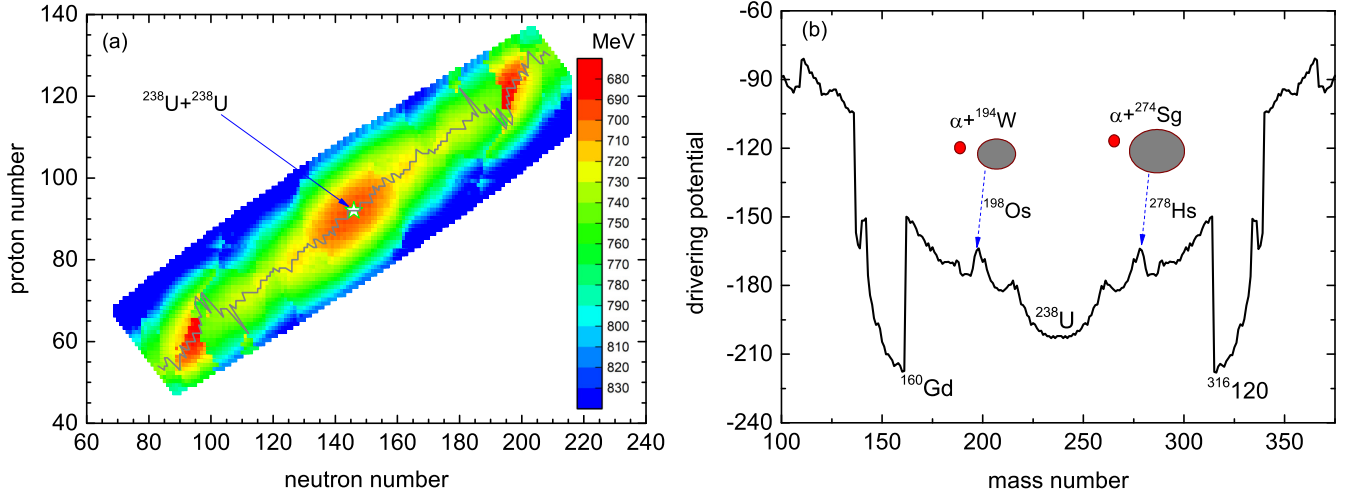


FIG. 1. (a) Potential energy surface as functions of proton and neutron numbers and (b) driving potential in the reaction of $^{238}\text{U} + ^{238}\text{U}$.

all possible DNS fragments within the dissipation of relative motion energy and angular momentum.

The level density is calculated from the Fermi-gas model [30] as

$$\rho(E^*, J) = \frac{2J + 1}{24\sqrt{2}\sigma^3 a^{1/4} (E^* - \delta)^{5/4}} \times \exp \left[2\sqrt{a(E^* - \delta)} - \frac{(J + 1/2)^2}{2\sigma^2} \right] \quad (17)$$

with $\sigma^2 = 6\bar{m}^2 \sqrt{a(E^* - \delta)}/\pi^2$ and $\bar{m} \approx 0.24A^{2/3}$. The pairing correction energy δ is set to be $12/\sqrt{A}$, 0 , $-12/\sqrt{A}$ for even-even, even-odd, and odd-odd nuclei, respectively. The level density parameter is related to the shell correction en-

ergy $E_{\text{sh}}(Z, N)$ and the excitation energy E^* of the nucleus as

$$a(E^*, Z, N) = \bar{a}(A) [1 + E_{\text{sh}}(Z, N) f(E^* - \Delta) / (E^* - \Delta)]. \quad (18)$$

Here, $\bar{a}(A) = \alpha A + \beta A^{2/3} b_s$ is the asymptotic Fermi-gas value of the level density parameter at high excitation energy. The shell damping factor is given by

$$f(E^*) = 1 - \exp(-\gamma E^*) \quad (19)$$

with $\gamma = \bar{a}/(\epsilon A^{4/3})$. The parameters α , β , b_s , and ϵ are taken to be 0.114, 0.098, 1, and 0.4, respectively [24].

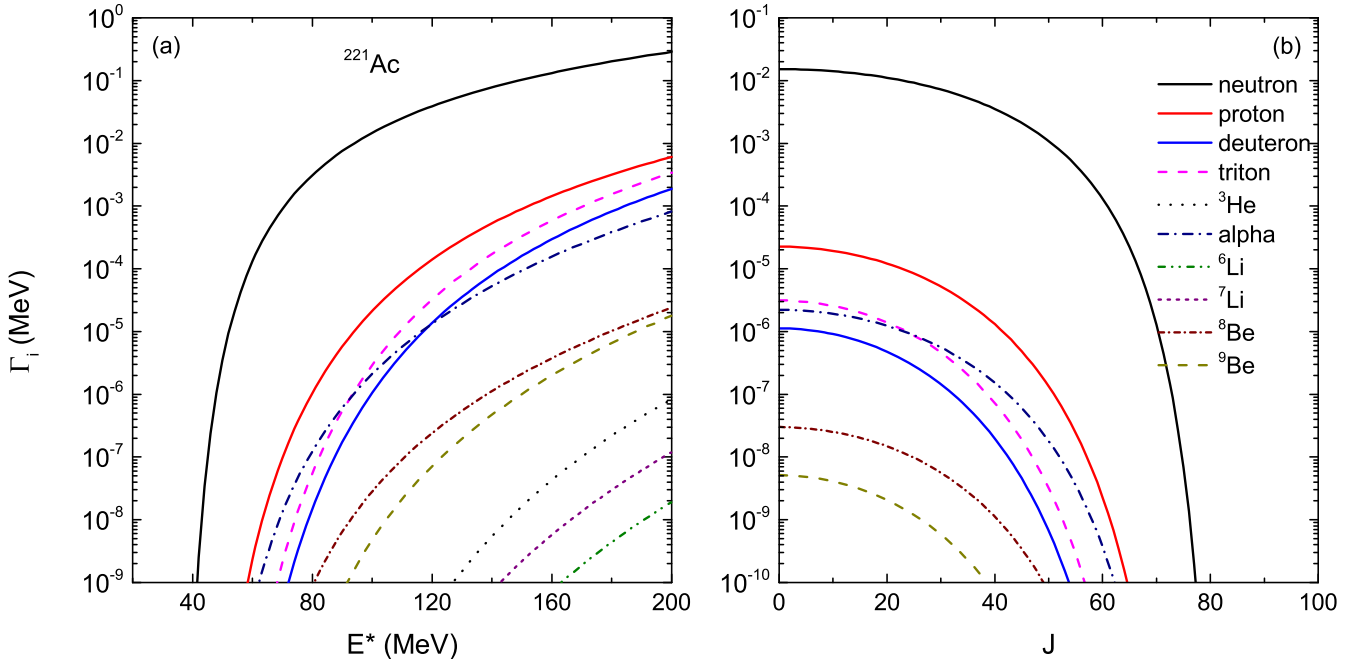


FIG. 2. Excitation energy and angular momentum dependence of partial decay widths of neutron, proton, deuteron, triton, ^3He , α , ^6Li , ^7Li , ^8Be , and ^9Be for the decay of ^{221}Ac which is formed in the reaction of $^{12}\text{C} + ^{209}\text{Bi}$.

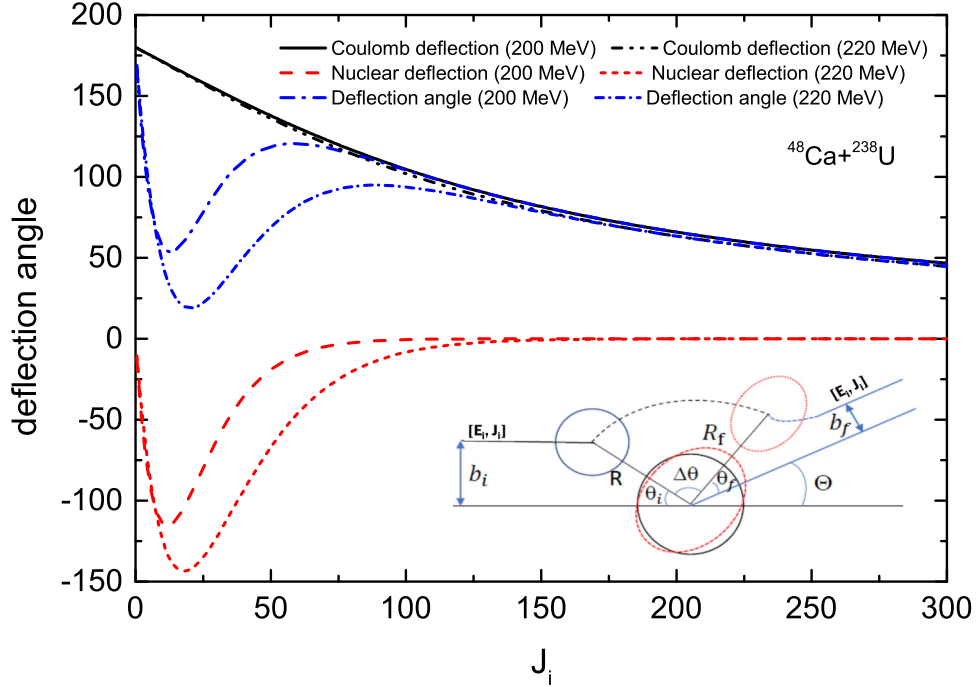


FIG. 3. The Coulomb and nuclear deflection angles as a function of angular momentum in the reaction of $^{48}\text{Ca} + ^{238}\text{U}$ at the center of mass energies of 200 and 220 MeV, respectively.

Once the emission probability of preequilibrium particle is determined, the kinetic energy is sampled by the Monte Carlo method within the energy range $\epsilon_v \in (0, E^* - B_v - E_{\text{rot}})$. The Watt spectrum is used for the neutron emission [31] and expressed as

$$\frac{dN_n}{d\epsilon_n} = C_n \frac{\epsilon_n^{1/2}}{T_w^{3/2}} \exp\left(-\frac{\epsilon_n}{T_w}\right) \quad (20)$$

with the width $T_w = 1.7 \pm 0.1$ MeV and normalization constant C_n . For the charged particles, the Boltzmann distribution is taken into account as

$$\frac{dN_v}{d\epsilon_v} = 8\pi E_k \left(\frac{m}{2\pi T_v}\right)^{1/2} \exp\left(-\frac{\epsilon_v}{T_v}\right). \quad (21)$$

The temperature of mother nucleus is given by $T_v = \sqrt{E^*/a}$ with the a being the level density parameter.

The polar angles of preequilibrium clusters emitted from the DNS fragments are calculated by the deflection function method, which is composed of the Coulomb and nuclear deflection as [25,32]

$$\Theta(J_i) = \Theta_C(J_i) + \Theta_N(J_i). \quad (22)$$

The Coulomb deflection is given by the Rutherford function as

$$\Theta(J_i)_C = 2 \arctan \frac{Z_p Z_t e^2}{2E_{c.m.} b} \quad (23)$$

with the incident energy $E_{c.m.}$ and impact parameter b . The nuclear deflection is calculated by

$$\Theta(J_i)_N = -\beta \Theta_C^{\text{gr}}(J_i) \frac{J_i}{J_{\text{gr}}} \left(\frac{\delta}{\beta}\right)^{J_i/J_{\text{gr}}}. \quad (24)$$

Here $\Theta_C^{\text{gr}}(J_i)$ is the Coulomb scattering angle at the grazing angular momentum J_{gr} and $J_{\text{gr}} = 0.22R_{\text{int}}[A_{\text{red}}(E_{c.m.} - V(R_{\text{int}}))]^{1/2}$. The J_i is the incident angular momentum. The A_{red} and $V(R_{\text{int}})$ are the reduced mass of projectile and target nuclei and interaction potential with R_{int} being the Coulomb radius, respectively. The parameters δ and β are parameterized by fitting the deep inelastic scattering in massive collisions as

$$\beta = 75f(\eta) + 15, \quad \eta < 375, \\ 36 \exp(-2.17 \times 10^{-3}\eta), \quad \eta \geq 375, \quad (25)$$

and

$$\delta = 0.07f(\eta) + 0.11, \quad \eta < 375, \\ 0.117 \exp(-1.34 \times 10^{-4}\eta), \quad \eta \geq 375, \quad (26)$$

with

$$f(\eta) = \left[1 + \exp\left(\frac{\eta - 235}{32}\right)\right]^{-1}. \quad (27)$$

The Sommerfeld parameter $\eta = \frac{Z_1 Z_2 e^2}{v}$ and the relative velocity $v = \sqrt{\frac{2}{A_{\text{red}}}(E_{c.m.} - V(R_{\text{int}}))}$. For the i -th DNS fragment, the emission angle is determined by $\Theta_i(J_i) = \Theta(J_i)\xi_i/(\xi_1 + \xi_2)$ with the moment of inertia ξ_i for the i -th fragment. Shown in Fig. 3 is a comparison of Coulomb deflection angle Θ_C and nuclear deflection angle Θ_N in the reaction of $^{48}\text{Ca} + ^{238}\text{U}$.

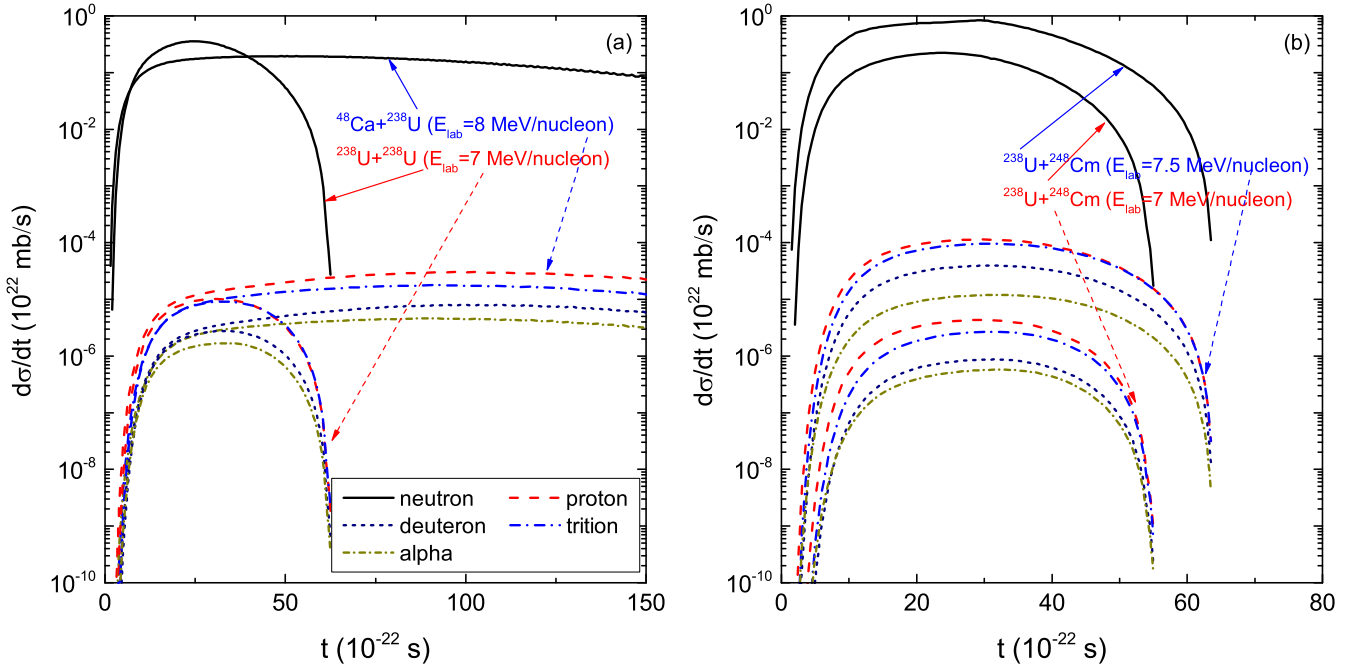


FIG. 4. Temporal evolution of the preequilibrium cluster emission in the reactions of $^{48}\text{Ca} + ^{238}\text{U}$, $^{238}\text{U} + ^{238}\text{U}$, and $^{238}\text{U} + ^{248}\text{Cm}$.

The Coulomb deflection is calculated by the well-known Rutherford scattering. The nuclear deflection is contributed from the attractive nuclear potential and the negative angle increases with the incident energy. Both the Coulomb and nuclear deflections influence the scattering angle in the projectile-target collisions. A schematic plot of the scattering process is also shown in the figure.

III. RESULTS AND DISCUSSION

The preequilibrium clusters in the transfer reactions are associated with the nuclear structure of collision partners, i.e., the preformation factor, stiffness of nuclear surface, binding energy, coupling strength of valence nucleons and core in weakly bound nuclide, etc., and also related to the reaction dynamics, i.e., the dissipation of relative motion and coupling to the internal degrees of freedom of reaction system. The preequilibrium cluster emission mechanism is also helpful for understanding the reaction dynamics of multinucleon transfer (MNT) process, e.g., the fragment cross section, total kinetic energy configuration, angular distribution, etc. Shown in Fig. 4 is the temporal evolution of the preequilibrium clusters produced in collisions of $^{48}\text{Ca} + ^{238}\text{U}$, $^{238}\text{U} + ^{238}\text{U}$, and $^{238}\text{U} + ^{248}\text{Cm}$ at the beam energies of 8, 7, and 7.5 MeV/nucleon, respectively. The configuration of emission rate is related with the reaction system and incident energy. The reaction of $^{48}\text{Ca} + ^{238}\text{U}$ leads to the formation of compound nucleus (copernicium) and undergoes the several hundreds of 10^{-22} s evolution. The local excitation energy of DNS increases with the reaction time and clusters might be continuously emitted during the fusion process. The probability is small and below 0.1%. The heavy systems $^{238}\text{U} + ^{238}\text{U}$ and $^{238}\text{U} + ^{248}\text{Cm}$ have the short interaction time and the clus-

ter emission rate manifests the maximal value at the time step of $20\text{--}40 \times 10^{-22}$ s. The neutron production in the reactions is dominant and the emission of hydrogen isotopes is comparable with alpha in magnitude. The maximal emission rates of the preequilibrium clusters in the reactions of $^{48}\text{Ca} + ^{238}\text{U}$ and $^{238}\text{U} + ^{238}\text{U}$ are similar but have different sustainable times. The preequilibrium emission is favorable with increasing incident energy.

It is well known that the emission of the MNT fragments is anisotropic and related to the reaction system and beam energy. The angular distribution of preequilibrium clusters is helpful for investigating the anisotropy of primary fragments in the MNT reactions. The sticking interaction time, moment of inertia, angular momentum, Coulomb and nuclear deflection of entrance system, etc., influence the emission angles of clusters corresponding to the collision orientation. We compared the angular distributions of the preequilibrium clusters produced in collisions of $^{238}\text{U} + ^{238}\text{U}$ and $^{238}\text{U} + ^{248}\text{Cm}$ at the beam energy of 7 MeV/nucleon as shown in Fig. 5. There exists a window with $60\text{--}110^\circ$ for the preequilibrium emission. The shape is very similar to the MNT fragments. The angular zone is nicely consistent with the preequilibrium α and ^8Be in experiments for the reaction of $^{12}\text{C} + ^{209}\text{Bi}$ at the beam energy of 73 MeV [2]. Accurate estimation of emission angle is helpful for managing the detector system in experiments. In this work, we treat the preequilibrium clusters emitted from the primary fragments in the MNT reactions. Neutron, proton, deuteron, triton, and alpha might be created with the same primordial nuclide.

The kinetic energy or momentum distributions of the preequilibrium clusters in transfer reactions manifest the internal structure of cluster inside the nucleus and are also associated with the reaction dynamics. The excitation of binary

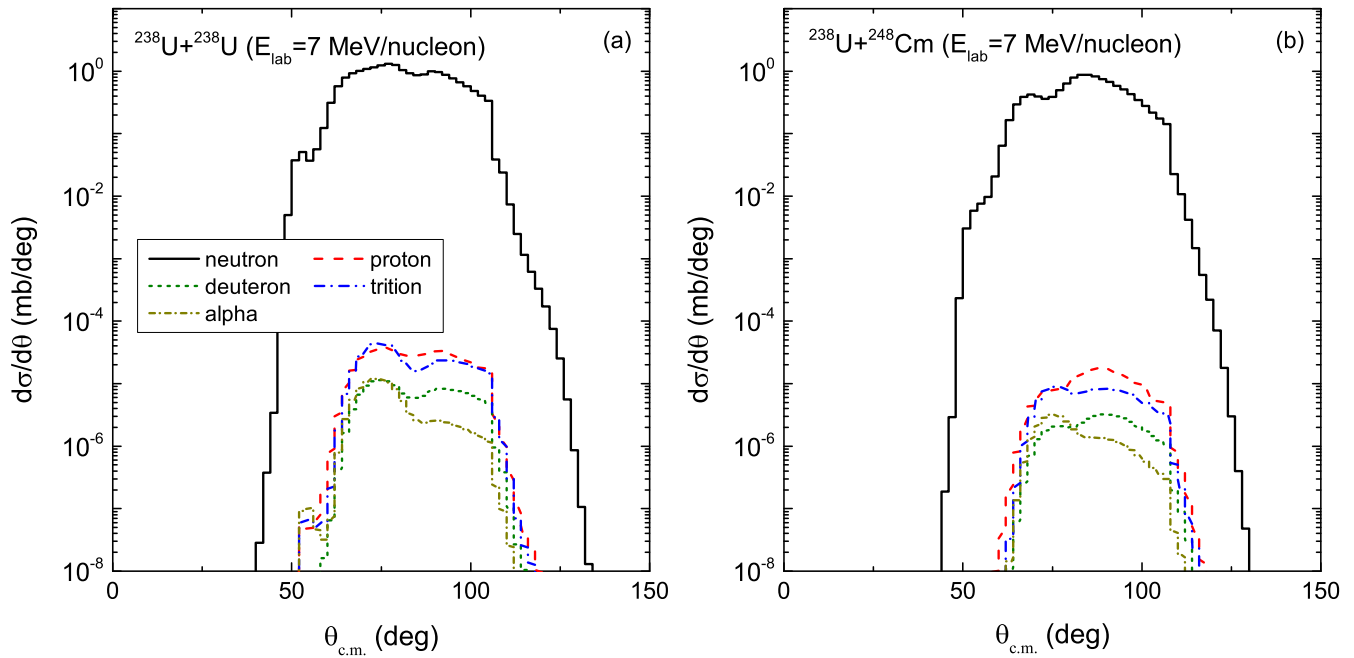


FIG. 5. Comparison of the angular distributions of the preequilibrium clusters produced in collisions of $^{238}\text{U} + ^{238}\text{U}$ and $^{238}\text{U} + ^{248}\text{Cm}$ at the beam energy of 7 MeV/nucleon.

nuclides, transition probability in nucleon transfer, binding energy, and separation energy of cluster influence the energy spectra. Shown in Fig. 6 is a comparison of the preequilibrium neutron, proton, deuteron, triton, and alpha produced in collisions of $^{238}\text{U} + ^{238}\text{U}$ and $^{238}\text{U} + ^{248}\text{Cm}$ at the incident energy of 7 MeV/nucleon. The clusters are emitted from the projectile-like or target-like fragments in the transfer reactions and manifest the Boltzmann distribution. The PES influences the local excitation energy of DNS and consequently con-

tributes the emission probability of preequilibrium clusters. It is obvious that the neutron emission is dominant and other particles are comparable in magnitude. The distribution structure is very similar to the kinetic energy spectra in high-energy proton induced spallation reactions [20]. The incident energy dependence of the preequilibrium clusters is shown in Fig. 7 for the angular distributions and kinetic energy spectra in the reaction of $^{238}\text{U} + ^{248}\text{Cm}$. The preequilibrium clusters at the energy of 7.5 MeV/nucleon are enhanced over the one-order

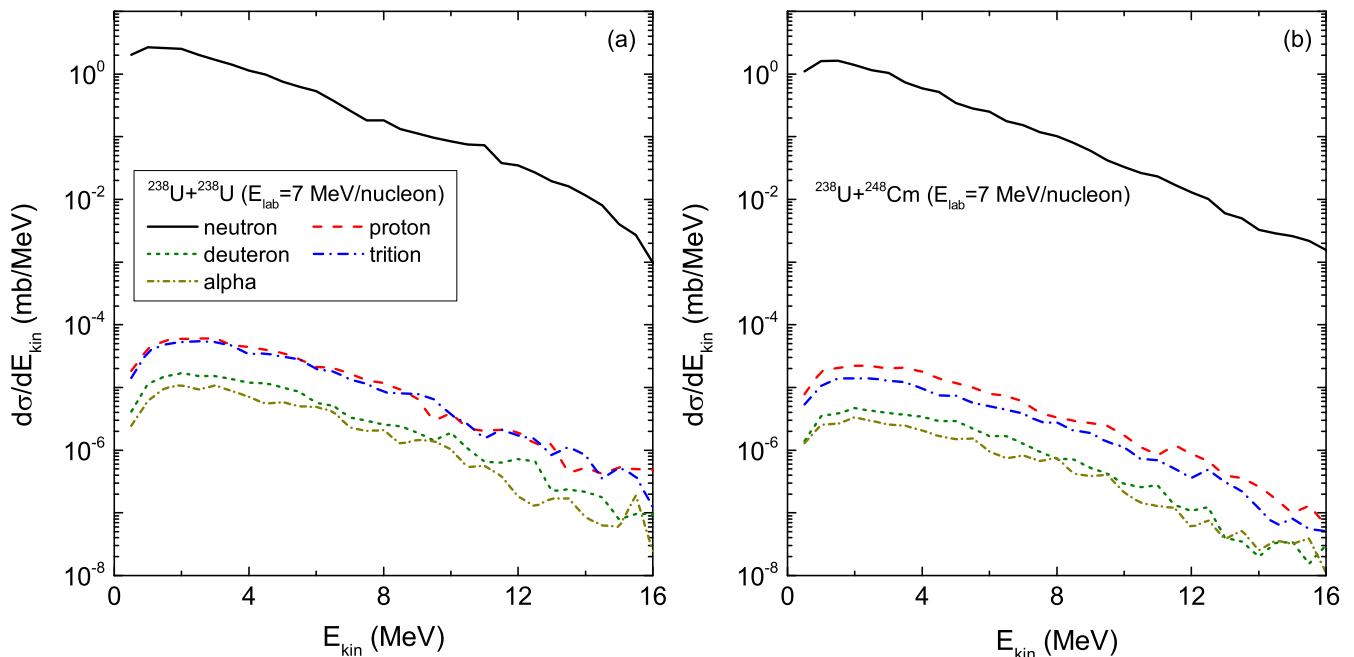


FIG. 6. Kinetic energy spectra of the preequilibrium clusters produced in collisions of $^{238}\text{U} + ^{238}\text{U}$ and $^{238}\text{U} + ^{248}\text{Cm}$.

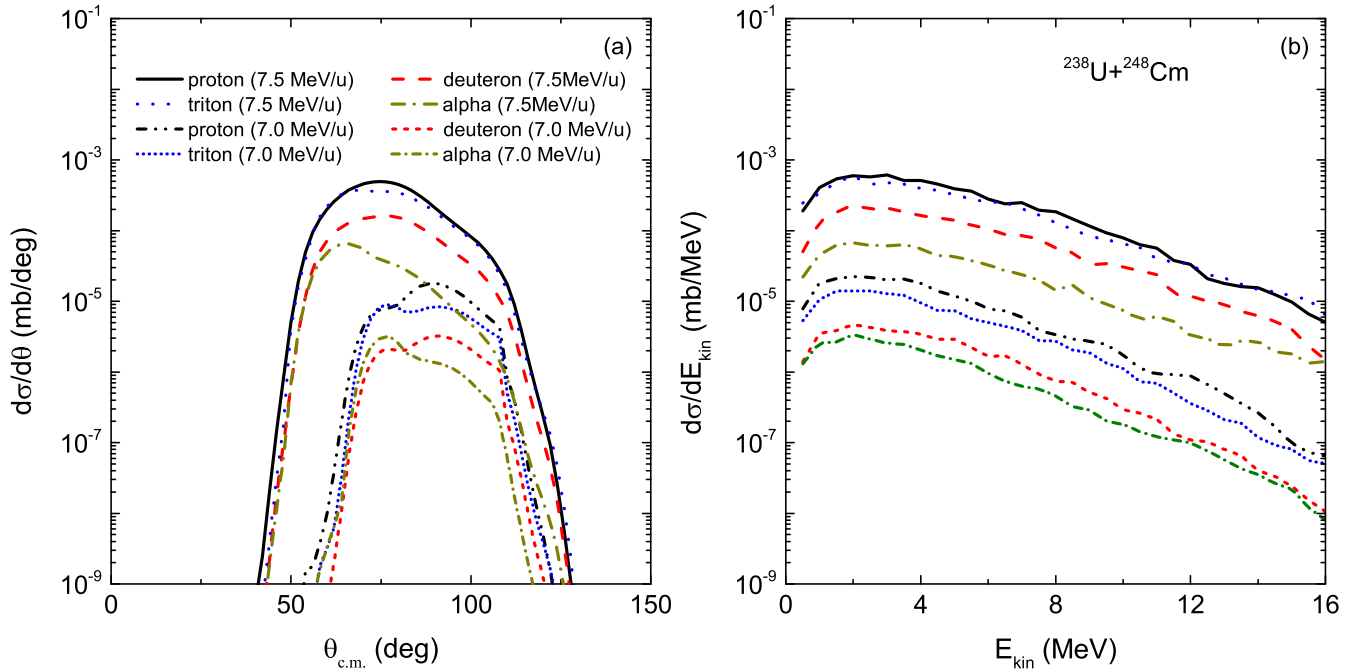


FIG. 7. (a) The angular distributions and (b) kinetic energy spectra of preequilibrium n , p , d , t , and α in the reaction of $^{238}\text{U} + ^{248}\text{Cm}$ at the beam energies of 7 and 7.5 MeV/nucleon, respectively.

magnitude and tend to the forward emission in comparison with the cases at 7.0 MeV/nucleon. We neglect the formation probability of cluster inside the DNS system and take the unit for all species of clusters. It has been known that the preformation of a cluster in single nucleus is described by the wave function method.

The cluster emission is associated with the nuclear structure and reaction dynamics. It provides information on the single particle and multinucleon correlation of nuclear states and might be used for exploring the nuclear spectroscopies.

The emission mechanism is different with the reaction system and beam energy. Shown in Fig. 8 is a comparison of the preequilibrium cluster production in the reactions of $^{40}\text{Ca} + ^{238}\text{U}$ and $^{48}\text{Ca} + ^{238}\text{U}$ at the center of mass energy 220 MeV. It is pronounced that the system $^{40}\text{Ca} + ^{238}\text{U}$ is favorable for the cluster production and has the broad energy and angular distributions. The total cross sections of preequilibrium neutron, proton, deuteron, triton, ^3He , α , ^7Li , and ^8Be produced in the transfer reactions of $^{12}\text{C} + ^{209}\text{Bi}$, $^{40,48}\text{Ca} + ^{238}\text{U}$, and $^{238}\text{U} + ^{238}\text{U}/^{248}\text{Cm}$ are listed in Table I. Three species can be

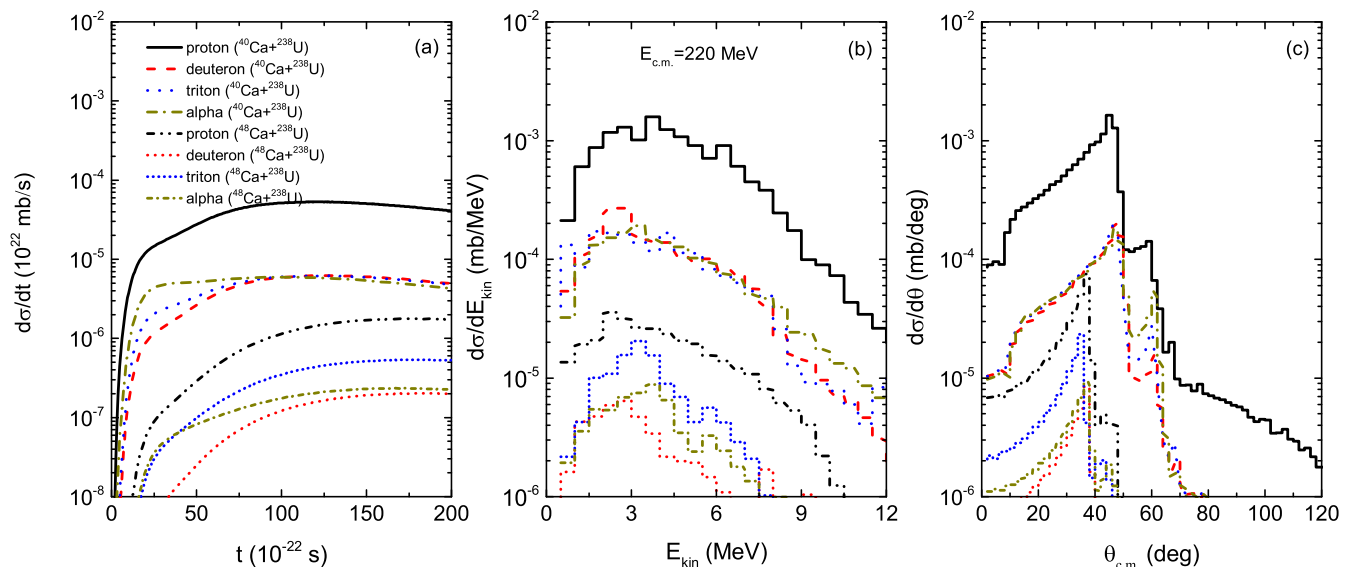


FIG. 8. Comparison of the production rate, kinetic energy spectra, and angular distributions of preequilibrium clusters in the reactions of $^{40}\text{Ca} + ^{238}\text{U}$ and $^{48}\text{Ca} + ^{238}\text{U}$ at the center of mass energy 220 MeV.

TABLE I. Production cross sections of neutron, proton, deuteron, triton, ^3He , α , ^7Li , and ^8Be in the preequilibrium process of massive transfer reactions.

System	$E_{c.m.}$ (MeV)	σ_n (mb)	σ_p (mb)	σ_d (mb)	σ_t (mb)	$\sigma_{^3\text{He}}$ (mb)	σ_α (mb)	$\sigma_{^7\text{Li}}$ (mb)	$\sigma_{^8\text{Be}}$ (mb)
$^{12}\text{C}+^{209}\text{Bi}$	69	2.63	0.26×10^{-3}	0.12×10^{-4}	0.41×10^{-4}	0.62×10^{-11}	0.22×10^{-3}	0.19×10^{-12}	0.42×10^{-12}
$^{40}\text{Ca}+^{238}\text{U}$	220	24.65	0.15×10^{-1}	0.17×10^{-2}	0.18×10^{-2}	0.62×10^{-8}	0.20×10^{-2}	0.16×10^{-10}	0.53×10^{-11}
$^{48}\text{Ca}+^{238}\text{U}$	180	0.11×10^{-1}	0.84×10^{-12}	0.21×10^{-14}	0.24×10^{-13}	$< 10^{-16}$	0.77×10^{-13}	$< 10^{-16}$	$< 10^{-16}$
$^{48}\text{Ca}+^{238}\text{U}$	200	1.63	0.42×10^{-5}	0.18×10^{-6}	0.66×10^{-6}	$< 10^{-16}$	0.54×10^{-6}	$< 10^{-16}$	$< 10^{-16}$
$^{48}\text{Ca}+^{238}\text{U}$	220	23.16	0.40×10^{-3}	0.44×10^{-4}	0.12×10^{-3}	0.23×10^{-11}	0.60×10^{-4}	0.74×10^{-14}	0.53×10^{-15}
$^{48}\text{Ca}+^{238}\text{U}$	240	96.11	0.61×10^{-2}	0.11×10^{-2}	0.28×10^{-2}	0.61×10^{-9}	0.94×10^{-3}	0.48×10^{-11}	0.34×10^{-12}
$^{238}\text{U}+^{238}\text{U}$	833	20.59	0.61×10^{-3}	0.17×10^{-3}	0.55×10^{-3}	0.49×10^{-10}	0.11×10^{-3}	0.15×10^{-11}	0.11×10^{-12}
$^{238}\text{U}+^{248}\text{Cm}$	850	11.53	0.23×10^{-3}	0.46×10^{-4}	0.14×10^{-3}	0.63×10^{-11}	0.31×10^{-4}	0.20×10^{-12}	0.16×10^{-13}
$^{238}\text{U}+^{248}\text{Cm}$	911	56.27	0.71×10^{-2}	0.24×10^{-2}	0.60×10^{-2}	0.41×10^{-8}	0.77×10^{-3}	0.10×10^{-9}	0.56×10^{-11}

classified according to the cross sections, the most probable emission for neutron, the medium for hydrogen isotopes and α with the 4–5 orders lower than the neutron emission, and the lowest probability for ^3He , ^7Li , and ^8Be production. The method is also possible for the weakly bound nuclei induced reactions with the inclusion of breakup probability.

IV. CONCLUSIONS

In summary, the emission mechanism of preequilibrium clusters in collisions of $^{12}\text{C}+^{209}\text{Bi}$, $^{40,48}\text{Ca} + ^{238}\text{U}$, $^{238}\text{U}+^{238}\text{U}$, and $^{238}\text{U}+^{248}\text{Cm}$ near Coulomb barrier energies has been systematically investigated within the DNS model. The preequilibrium clusters are considered to be emitted from the decay of the primordial DNS fragments in the nucleon transfer process. The production rate is associated with the reaction system and beam energy. The preequilibrium emission takes place until the formation of compound nucleus. The kinetic spectra manifest the Boltzmann shape. The angular distribution is similar to the transfer fragments, i.e., in the

range 70–110° for the reactions of $^{238}\text{U}+^{238}\text{U}/^{248}\text{Cm}$ and forward emission 35–60° for the light systems of $^{40,48}\text{Ca} + ^{238}\text{U}$. The production cross sections of preequilibrium clusters strongly depend on the separation energy and Coulomb barrier from the primordial nuclides. The neutrons are emitted and also take away the local excitation energy of the DNS system. The emission rate of alpha and hydrogen isotopes is comparable in the magnitude. The production of heavier clusters, such as lithium, beryllium isotopes, etc., are associated with the reaction system. The method is also possible for describing the weakly bound nuclei induced reactions after including the nuclear structure effects, e.g., the preformation probability of cluster, coupling of valence nucleons, or cluster to the core nucleus, etc.

ACKNOWLEDGMENTS

This work was supported by the National Natural Science Foundation of China (Projects No. 12175072 and No. 11722546) and the Talent Program of South China University of Technology (Projects No. 20210115).

[1] P. E. Hodgson and E. Běták, *Phys. Rep.* **374**, 1 (2003).
 [2] G.-M. Jin, Y.-X. Xie, Y.-T. Zhu, W.-G. Shen, X.-J. Sun, J.-S. Guo, G.-X. Liu, J.-S. Yu, C.-C. Sun, and J. D. Garrett, *Nucl. Phys. A* **349**, 285 (1980).
 [3] Z. Lewandowski, E. Loecer, R. Wagner, H. H. Mueller, W. Reichart, and P. Schober, *Nucl. Phys. A* **389**, 247 (1982).
 [4] S. S. Dimitrova, G. Z. Krumova, P. E. Hodgson, V. Avrigeanu, and A. N. Antonov, *J. Phys. G* **23**, 961 (1997).
 [5] A. A. Cowley, G. F. Steyn, S. S. Dimitrova, P. E. Hodgson, G. J. Arendse, S. V. Förtsch, G. C. Hillhouse, J. J. Lawrie, R. Neveling, W. A. Richter, J. A. Stander, and S. M. Wyngaard, *Phys. Rev. C* **62**, 064605 (2000).
 [6] C. M. Herbach *et al.*, *Nucl. Phys. A* **765**, 426 (2006).
 [7] A. Budzanowski *et al.*, *Phys. Rev. C* **78**, 024603 (2008).
 [8] A. G. Artukh, V. V. Avdeichikov, G. F. Gridnev, V. L. Mikheev, V. V. Volkov, and J. Wilczynski, *Nucl. Phys. A* **176**, 284 (1971).
 [9] A. G. Artukh, G. F. Gridnev, V. L. Mikheev, V. V. Volkov, and J. Wilczynski, *Nucl. Phys. A* **211**, 299 (1973).
 [10] K. D. Hildenbrand, H. Freiesleben, F. Philhofer, W. F. W. Schneider, R. Bock, D. V. Harrach, and H. J. Specht, *Phys. Rev. Lett.* **39**, 1065 (1977).
 [11] W. von Oertzen, M. Freer, and Y. Kanada-En'yo, *Phys. Rep.* **432**, 43 (2006).
 [12] L. F. Canto, P. R. S. Gomes, R. Donangelo, and M. S. Hussein, *Phys. Rep.* **424**, 1 (2006).
 [13] F. Iachello and A. D. Jackson, *Phys. Lett. B* **108**, 151 (1982).
 [14] F. A. Janouch and R. J. Liotta, *Phys. Rev. C* **27**, 896 (1983).
 [15] W. T. Pinkston, *Phys. Rev. C* **29**, 1123 (1984).
 [16] M. Blann, *Annu. Rev. Nucl. Sci.* **25**, 123 (1975).
 [17] E. Gadioli, E. Gadioli Erba, and J. J. Hogan, *Phys. Rev. C* **16**, 1404 (1977).
 [18] O. V. Fotina, D. O. Eremenko, Yu. L. Parfenova, S. Yu. Platonov, and O. A. Yuminov, *Int. J. Mod. Phys. E* **19**, 1134 (2010).
 [19] Y. Jia and J.-D. Bao, *Phys. Rev. C* **75**, 034601 (2007).
 [20] H. G. Cheng and Z. Q. Feng, *Chin. Phys. C* **45**, 084107 (2021).
 [21] V. V. Volkov, *Phys. Rep.* **44**, 93 (1978).
 [22] Z. Q. Feng, G. M. Jin, F. Fu, and J. Q. Li, *Nucl. Phys. A* **771**, 50 (2006).
 [23] Z. Q. Feng, G. M. Jin, J. Q. Li, and W. Scheid, *Phys. Rev. C* **76**, 044606 (2007); *Nucl. Phys. A* **816**, 33 (2009).

- [24] Z. Q. Feng, G. M. Jin, and J. Q. Li, *Phys. Rev. C* **80**, 067601 (2009); Z. Q. Feng, *ibid.* **95**, 024615 (2017).
- [25] G. Wolschin and W. Nörenberg, *Z. Phys. A* **284**, 209 (1978).
- [26] J. Q. Li and G. Wolschin, *Phys. Rev. C* **27**, 590 (1983).
- [27] V. Weisskopf, *Phys. Rev.* **52**, 295 (1937).
- [28] P. H. Chen, Z. Q. Feng, J. Q. Li, and H. F. Zhang, *Chin. Phys. C* **40**, 091002 (2016).
- [29] P. Möller, J. R. Nix, W. D. Myers, and W. J. Swiatecki, *At. Data Nucl. Data Tables* **59**, 185 (1995).
- [30] A. S. Iljinov, M. V. Mebel, N. Bianchi, E. De Sanctis, C. Guaraldo, V. Lucherini, V. Muccifora, E. Polli, A. R. Reolon, and P. Rossi, *Nucl. Phys. A* **543**, 517 (1992).
- [31] H. Rossner, D. J. Hinde, J. R. Leigh, J. P. Lestone, J. O. Newton, J. X. Wei, and S. Elfstrom, *Phys. Rev. C* **45**, 719 (1992).
- [32] C. Peng and Z. Q. Feng, *Eur. Phys. J. A* **58**, 162 (2022).